Empirical Derivation of a Nusselt Number in a Thermally Stratified Enclosure

Izumi Hagiwara[1], A. Tokuhiro[2], P. G. Oduor[3],*

Abstract

A hydrophilic gelatin suspension possesses thermal properties that may affect the ratio of convective to conductive heat transfer across a boundary. This ratio, also known as Nusselt's number, can represent laminar or turbulent flow regimes. In this study, thermal transitioning empirical values were determined using a gelatin as a polymer gel surrogate. The crux of this study was to (a) quantify heat transfer properties of the gelatin as a suspended semi-solid and (b) understand thermal profiles with respect to particle size and loading. We can adduce the existence of a thermally induced: lower rise velocity, stratified Nusselt number, and a boundary layer.

Keywords: Hydrophilic particle; single-phase; two-phase flow.

[1] Formerly at University of Missouri-Rolla (Missouri University of Science and Technology), Nuclear Engineering Department, Missouri University of Science and Technology, 222 Fulton Hall, 301 W. 14th St., Rolla, MO 65409-0170 (h19_izumi@hotmail.com)
[2] Akira Tokuhiro, Faculty of Energy Systems and Nuclear Science, Energy Systems and Nuclear Science Research Centre (ERC), Room 4036, North Oshawa, 2000 Simcoe Street North, Oshawa, ON L1H 7K4, Canada (akira.tokuhiro@uoit.ca)
[3] Dept. of Geosciences, North Dakota State University, Fargo, ND 58108 (Peter.Oduor@ndsu.edu)
*Corresponding Author

Introduction

The importance in understanding comparative heat transfer between single and liquid-solid phase transition can be seen in potential applications especially in dynamic filtering. Hoffman et al. [1-2], Hoffman [3], and Cui et al. [4] showed that gels could be used to: (i) remove undesirable compounds, (ii) improve the quality of metals, and (iii) improve biochemical processes. Focusing only on the hydrophilic nature of a gel, natural convection [5, 6] of a temperature sensitive gel suspension can be simulated as a natural convection of a hydrophilic particle suspension. Hydrophilic particles even though insoluble in water may be considered to include those that may absorb and retain water in various proportions. In cases where the solid phase is micron-sized, hydrophilic particles tend to settle out of suspension. Such behavior of particles and their hydrophilic property appear to have some influence on heat transfer mechanisms of single-phase natural convection. In a typical single-phase flow, there exists only the fluid that flows owing to a generated temperature gradient. In a two-phase flow, a second phase has the chance of moving with the convective flow and settling out if the density of the material exceeds that of the fluid phase.

In many naturally occurring situations, fluid motion results from variations in the buoyancy force, which is a consequence of horizontal temperature gradients in the fluid. This has led to theoretical and experimental studies on the role played by buoyancy forces in a variety of circumstances. Previous studies were focused on either details of the motion of the fluid and of the temperature distribution within the fluid or the rate of transfer of heat across the cavity. To find the rate of heat transfer, details of the fluid motion and temperature distribution was determined. The main problem occurs in delineating a simple workable geometry of the convection cell. Accommodations are usually made to simplify geometries and assess relevance of the overall picture than to a particular geophysical situation. Batchelor [7] published an analytical study of natural convection in enclosed gas layers formulated in a 2D (two-dimensional) form, which has since been expanded to address natural convective flow in 3D. In this case, a fluid of kinematic viscosity, v, thermal diffusivity, α, and with coefficient of thermal expansion, β, fills a rectangular cavity bounded by two vertical walls, distance L apart, and two horizontal walls, distance H apart. If the two vertical walls are maintained at different temperatures, that is, T_{hot} (heated wall) and T_{cold} (cooled wall) then the Rayleigh number, Ra, can be calculated from, $Ra = \left(g\beta\Delta TH^3/\nu\alpha\right)$, where g is the acceleration due to gravity, ΔT is the representative temperature difference in the system. ΔT can be either the difference between hot and cold wall temperature, $T_{\text{hot}} - T_{\text{cold}}$, or the difference between hot wall temperature and the bulk temperature of the fluid in the cell, $T_{\text{hot}} - T_{\text{bulk}}$, accordingly. Prandtl number, Pr, is obtained from $\text{Pr} = (\nu/\alpha)$, and the aspect ratio A defined as, $A = (H/L)$, where L is the distance between hot and cold walls. Several flow regimes exist dependent on Ra and A [7]. Free convection heat transfer can be enhanced using, for example; an electric field [8], additives [9], ideal spacer grids [10], improved rib turbulators [11], or even finned microchannels [12].

The dichotomy of flow and temperature distribution plays a role in ascertaining any flow regime. This can best be described from Eckert and Carlson [13] and Elder [14] studies on temperature fields that can be evaluated using Zehnder-Mach interferograms. The apparatus used in their experiments could be assembled with aspect ratios from 2:1 to 46:7 and the temperature difference between the vertical walls varied between $10\ ^\circ\text{F}$ and $160\ ^\circ\text{F}$. The selection of widths and temperature differences used enable the Rayleigh number to be varied from approximately 200 to 2×10^5. As predicted by Batchelor [7] and Eckert and Carlson's [13] experimental results showed that below a certain Rayleigh number and above a certain aspect ratio, heat was transferred from the hot to the cold wall by conduction, with convection effects restricted to the corner regions. However, in a boundary layer regime (above a certain *Ra* and below a certain *A*) the temperature was uniform along horizontal lines only and increased in the vertical direction. The various flow regimes are delimited by Eckert and Carlson [13] and are also shown by Ostrach [15] in terms of the range of Grashof, *Gr* (i.e. $Gr = Ra/\mathrm{Pr}$), numbers and aspect ratio values.

Experiments that further support the stratified core configuration are reported by Elder [14]. Velocity measurements, made by direct observation of aluminum powder suspended in the fluid, were obtained in addition to temperature measurements [14]. The fluids were medicinal, paraffin and silicone oil, which have Prandtl numbers near 1000 [14]. The upper cavity was open to the environment (air) so that thermocouples could be inserted. He observed the existence of steady multicellular flows (secondary and tertiary flows). Seki et al. [16] studied experimental visualization of natural convective flow in a narrow vertical cavity using several kinds of fluid and investigated the effects of the Prandtl number and the cavity width on the flow pattern. They obtained experimental measurements for net heat transfer through the vertical fluid layer for aspect ratios of 6-30 and Prandtl numbers of 4-12500.

Guided by the experiments of Elder [14] a theoretical model was developed by Gill [17] for the limitations of large Prandtl numbers. A number of numerical solutions for the vertical cavity problem were obtained by de Vahl Davis [18], MacGregor and Emery [19], Newell and Schmidt [20], Luz Neto [21, 22], and Mavromatidis [23]. A comparison of various solutions is presented by de Vahl Davis [18] and Ostrach [15]. They formulated a correlation equation and from their results, permitted reasonable predictions of heat transfer over a range of conditions. A more comprehensive review of numerical methods for natural convection in rectangular cavities is presented by de Vahl Davis [24].

A variety of theoretical expressions, graphical correlations, and empirical equations have been developed to represent the coefficients for heat and mass transfer by free convection from vertical plates. Nusselt number, *Nu*, is a dimensionless parameter that represents the temperature gradient at a surface where heat is transferred from a heated wall to fluid [25, 26]. It is also interpreted as ratio of convection heat transfer to fluid conduction heat transfer under the same conditions. Explicit expressions for Nusselt number pertaining to free convection are well known from dimensional analysis, scaling, and actual experiments [27]. The Nusselt number, *Nu*, is a function of the Rayleigh number *Ra*, or Grashof number *Gr*. Empirical expressions have been derived by Churchill and Usagi [28], Churchill and Ozoe [29], and Churchill and Chu [30] and a comprehensive review is presented by Churchill [31].

When thermal stratification occurs, the fluid is spatially confined while it is heated or cooled [32, 33]. The strength of stratification is measured by the stratification parameter, *S*, defined as $S = (T_{\mathrm{top}} - T_{\mathrm{bottom}})/(T_{\mathrm{wall}} - T_{\mathrm{bulk,y}})$, where T_{top} and T_{bottom} are, respectively, the bulk temperature at the top and bottom of the heated section and T_{wall} and $T_{\mathrm{bulk,\,y}}$ are, respectively, the wall and bulk temperatures. The *S* value in the non-stratified case, assumes a value of zero. Lykoudis and Tokuhiro [34] investigated bulk temperature stratification using order-of-magnitude analysis.

Heat transfer for two-phase introduces various complexities [1-3]. Comparatively in dynamic filtration, we can assess enhancement-de-enhancement properties for different particle loadings to determine an optimal threshold in filtration. The main focus of this study was to investigate feasibility of a gelatin suspension in deionized water as a probable dynamic filter candidate by examining its thermal properties.

Methods

Gelatin, a water-absorbing (hydrophilic) particle, with a swelling property and density close to water when hydrated was used. With a diameter between 50 and 200 µm, it can be adequately tracked using an acoustic velocity analytic instrument. We ascertained its dry bulk density ≈ 680 kg/m^3 and wet density ≈ 1390 kg/m^3 using Archimede's principle. It has been reported elsewhere that the wet density of gelatin is about 1270 kg/m^3 (e.g. [35]). Its solubility is limited below the boiling point of water. Using a sieve shaker and four sets of sieves, the gelatin particles were fractionated into four different sizes with particle diameter ranges, 125-150 µm, 75-125 µm, 45-75 µm, < 45 µm, whose median particle diameter was used as the defining size except for the < 45 µm size fraction which was recorded as 45 µm size class. These classes were further reclassified using their representative Martin's diameters (e.g. [36-38]). Martin's diameter is the smallest diameter measured between opposite sides of a particle, and determined in a direction transverse to the particle on a line that bisects the projected area considering all possible directions [36-38]. Martin's diameters were measured with an SMZ800 Nikon microscope. Particle imagery was obtained using a digital camera. A custom Plexiglas enclosure was filled with ≈ 20 liters of distilled and deionized water for each run. For gelatin particle measurements, tracer particles (Expancel microspheres (091 DU 80, Akzo Nobel) were added to the experiment container. These were added to the dual-phase flows after temperature measurements were taken.

The Plexiglas enclosure (Height = 106.7 cm, Width = 61 cm, Thickness = 0.943 cm) with aluminum and PVC square channels sandwiched between them. The Plexiglas sheets were further insulated with polystyrene. The aluminum with a higher thermal conductivity, lined the inner side of the cell at the heated and cooled sidewalls. The lower conducting PVC channels lined the outer exposed side, including the bottom of the enclosure. All immovable parts were held together using a clear, waterproof adhesive (UV6800, Eclectic Products, Inc.). The system temperature was controlled by two 6-liter constant temperature dual refrigerator-heater LAUDA RM6 Brinkman Instruments circulating baths connected by insulated aluminum tubes. Water flowed initially downward from the aluminum channel into the connected PVC channel. Water also flowed secondarily from the PVC channel to the circulating bath (Fig. 1). Ten Chromel-Alumel thermocouples (36 AWG) at 10.16 cm from each other were attached along the entire wall surface using a 0.05 mm thick aluminum tape. The temperature inside the test cell was determined by a moveable thermocouple unit, which consisted of ten Chromel-Alumel 20 AWG calibrated thermocouples in plastic tubes. Temperature difference was gauged using a dual setup with 32 AGW Chromel-Alumel thermocouples attached to the hot end wall compared to 20 AGW Chromel-Alumel thermocouples for the cold end were utilized. The hot wall temperature (T_{hot}) was determined from differential temperature of the inside and surface of the transfer tube. Heat flux was thereafter calculated using Fourier's law of heat conduction.

Bath temperature values of 10°C and 20°C were set as in our previous studies (i.e. [39, 40]), mainly to compare between single and dual phases for gelatin particle sizes (d_1 = 134 μm, d_2 = 230 μm) and loadings (ϕ_1 = 0.026 wt%, ϕ_2 = 0.104 wt%, ϕ_3 = 0.26 wt%, ϕ_4 = 0.518 wt%). Standard tables (e.g. [41]) were used for other thermophysical properties not empirically determined, for example, viscosity. The cell was emptied, cleaned, and refilled with deionized and degassed water. After initiating the water baths, temperature was measured every half an hour. All temperature measurements were aptly synchronized and determined concurrently via a data logger (Data Acquisition System - Personal Daq, IOtech). This was done until steady-state (~ 6 hours) was attained, that is, when thermal fluctuation did not exceed 0.2°C. Cold wall temperatures, on the other hand, were determined every quarter of an hour. Before a set loading of gelatin particles was introduced into the cell, the mixture was thoroughly dispersed using a magnetic stirrer. Sediment layer depth and morphology was also determined. Temperature measurement from the roving thermocouple probe was obtained using a 54II FLUKE thermocouple thermometer.

Sediment layer depth was measured during the experimental runs for two-phase natural convection. Sedimentation occurred due to a density of some gelatin particles greater than that of water. The time taken for each particle to sink to the bottom of the convective cell depends on particle size. Consequently, the particles sank to the bottom gradually since there was a particle size distribution. The sediment layer depth increased with time before slowing down after about three hours.

Error analysis

Quintuplicate data was taken for each experimental run as described in [39, 40] and an error analysis was performed for the following empirically derived variables: (i) temperature (T), (ii) local Nusselt number (Nu_y), and (iii) local Rayleigh number, (Ra_y) [40]. Standard error values were generated for all temperature measurements. The error in $\left(dT/dx\right)\big|_{x=0}$ was obtained using linear-to-cubic polynomial regression equations. The final relative error in the local Nusselt number, Nu_y, determined using error propagation was [40]:

$$\frac{\sigma_{m,Nu_y}}{Nu_y}=\sqrt{\left(\frac{\sigma_{m,T_{\text{hot, y}}-T_{\text{x}}}}{T_{\text{hot, y}}-T_{\text{x}}}\right)^2+\left(\frac{\sigma_{m,T_{\text{hot, y}}-T_{\text{bulk, y}}}}{T_{\text{hot, y}}-T_{\text{bulk, y}}}\right)^2+\left(\frac{\sigma_{m,y}}{y}\right)^2+\left(\frac{\sigma_{m,x}}{x}\right)^2} \quad (1)$$

Where T_x is the temperature at one millimeter from the hot wall, x the distance from the hot wall, and, y, the thermocouple position at each height. The standard errors were calculated for the hot wall temperature, $T_{\text{hot},y}$, bulk temperature of the cell, $T_{\text{bulk},y}$, and temperature from the hot wall surface, T_x. The standard error of the temperature difference was calculated from $\sigma_{m,T_{\text{hot, }y}-T_x}=\sqrt{\left(\sigma_{m,T_{\text{hot, }y}}\right)^2+\left(\sigma_{m,T_x}\right)^2}$, where σ_m indicates the standard errors for $T_{\text{hot},y}$ and T_x.

Results and discussion

Fig. 2 shows a schema of the trajectory of gelatin particles prior to sedimentation depending on aspects including hydrated density, hydrated size, and shape. The larger-sized particles traced a path (path (c)) much closer to the hot end than the lighter particles. The intermediate-sized particles followed a trajectory illustrated by (b) whereas the lightest particles followed (a). The maximum sediment thickness, D_{max}, was determined closer to the hot end. The mean sediment layer depth corresponded to a height that the same area of sediment profile would occupy when fully spread along the bottom of the cell. The results were then tabulated. The values were for 9$^{\text{th}}$ to 20$^{\text{th}}$ run that corresponds to the two-phase natural convection cases. Table 1 shows values measured for the mean sediment layer depth for each experimental run for the two-phase flow case. The mean sediment layer was determined by taking the average values for different positions for each run. For 9$^{\text{th}}$ and 10$^{\text{th}}$ experimental run, the sediment layer depth was measured only at center of the experimental cell and thus, the mean sediment layer depth was not obtained. The mean sediment layer is higher for the bath temperature difference of 10°C than for 20°C except for case of particle size of 230 mm and particle loading of 0.260 wt%. The mean sediment layer depth becomes higher when the particle load is increased. With a bath temperature difference of 10ºC and particle loading of 0.260 wt%, the mean sediment layer depth is higher for smaller particle size [39, 40], whereas it was converse for bath temperature difference of 20ºC and particle loading of 0.260 wt%. The highest value for the mean sediment thickness was 11.3 cm for the 15th run when the temperature of the water bath was 10ºC. The lowest value was 1.2 cm when water bath temperature was 20ºC corresponding to the 18th experimental run.

Figure 3 shows temperature profiles of single-phase and two-phase cases at 3.0 cm from the bottom of the cell, where sediment layer is seen for two-phase case. The bath temperature difference is 10°C. The sediment layer depth for two-phase case was 11.3 cm. The measurement points were from one millimeter from the hot wall to 300 mm from the hot wall, which is about centerline between the hot and cold walls. The measured temperature is plotted against the distance from the hot wall. In the two-phase flow case the trend does not have a steep gradient. This indicates that conduction heat transfer predominates much more than the expected convective curve for single phase. The "conduction line" in Fig. 3 indicates the temperature profile of the conduction regime (e.g. [13]), which is defined as heat transferred by only conduction (conduction regime). For the case of single-phase natural convection, the temperature is constant along a horizontal line in the central part of the cell and the temperature gradient is concentrated in the layer adjacent to the hot wall (boundary layer). However, for the case of the two-phase natural convection, the temperature is not constant in the central part of the cell, but gradually decreases towards the cold wall. Consequently, the temperature gradient at the hot wall is smaller and the bulk temperature is higher compared to single-phase case.

Due to thermal stratification of the ambient fluid within the cell, the wall temperatures were not constant (Fig. 4). Thermal stratification is characterized by warm fluid layers on top of gradually colder layers. This thermal stratification of fluid within the cell appears to affect the wall temperature distribution. That is, the wall temperature at the top of the cell will have higher temperature than at the bottom of the cell. The hot wall temperature was measured by using a thermometer (54 II, FLUKE), whose measurement accuracy was about ±0.33°C. The cold wall temperature was measured and recorded by a data acquisition module (Personal Daq/56, IOtech) with a thermocouple accuracy was ±0.4°C. The temperatures were measured every fifteen or thirty minutes during each run (≈ 2 hours) until steady state. The wall temperatures are averaged over the experimental period and shown in Figure 4. From Fig. 4, the hot wall temperature was higher at the top of the convective cell than at the bottom as expected. This was not the case with the cold wall. The hot and cold walls were heated or cooled by letting water circulate through the aluminum channel from top to bottom of the cell. At the hot wall end, the heated water temperature is gradually decreased due to colder fluid within the cell. This temperature gradient of the hot wall was the same as the temperature gradient of ambient fluid within the cell due to thermal stratification. On the other hand, at the cold wall; the cooled water temperature was gradually increased due to thermally high fluid within the cell. This temperature gradient of the cold wall was opposite to that of the ambient fluid within the cell caused by thermal stratification. That is probably why the cold wall temperature did not display the same trend as the hot wall temperature variation.

Table 2 shows the maximum wall temperatures for the hot and cold walls and percent difference determined from the ratio of the difference in maximum and minimum temperatures for each wall to the mean temperature in percentage. $\overline{T}_{\text{hot}}$ is average hot wall temperature,

$T_{\text{h, max}}$ is the maximum hot wall temperature, $T_{\text{h, min}}$ is the minimum hot wall temperature, and ΔT_{h} is the temperature difference between the maximum and minimum hot wall temperatures. $\overline{T}_{\text{cold}}$ is average cold wall temperature, $T_{\text{c, max}}$ is the maximum cold wall temperature, $T_{\text{c, min}}$ is the minimum cold wall temperature, ΔT_{c} is the temperature difference between the maximum and minimum cold wall temperatures. The difference is calculated from the relation: $\left\{\left(T_{\text{h, max}} - T_{\text{h, min}}\right)/\overline{T}_{\text{hot}}\right\} \times 100$.

Figs. 5 and 6 show temperature contours in 2D for both single-phase and dual-phase natural convection. Temperature contours for the single-phase and two-phase natural convection were derived from temperature measurements along vertical (H) and horizontal (L) axes as depicted in Figure 1. The dimensionless values were derived from the relation $\left(T - T_{\text{cold}}\right)/\left(T_{\text{hot}} - T_{\text{cold}}\right)$, where T is the local temperature, T_{cold} is cold wall temperature, and T_{hot} is hot wall temperature. x is distance measured from the hot end, and L is the entire cell width. Higher values of x/L (unitless) indicate distances further away from the hot wall. Fig. 5 shows temperature profiles for single- and dual-phase flows for 134 μm particles. The upper row depicts bath temperature difference of 10°C while the lower is for 20°C difference at ($0 \leq x/L \leq 0.02$). Thermal stratification can be seen in Fig. 5 with a general lower right cooler end. With higher weight loadings, the thermal layer laterally migrates towards the lower portions at higher x/L values. It is also worthwhile to note that the 0.4 contour line reaches a maximum with weight loadings from $\phi_p = 0.026$ wt% to $\phi_p = 0.260$ wt% but diminishes drastically at $\phi_p = 0.518$ wt%. In Fig. 6, for $0 \leq x/L \leq 0.02$, the effect of particle loading and ΔT_{Bath} can be observed. The top row shows contours for $\Delta T_{\text{Bath}} = 10$°C and the bottom row shows for $\Delta T_{\text{Bath}} = 20$°C. Again the thermal profile in this case displays a similar trend as in Fig. 5 for $\phi_p = 0.260$ wt%. The thermal contours for ϕ_p = 0.026 wt% are remarkably different. At a closer look, however, the 0.4 contour line starts off at a lower *y*/*H* for ΔT_{Bath} = 10˚C and ϕ_p = 0.260 wt% compared to when ΔT_{Bath} = 20˚C. For ΔT_{Bath} = 20˚C and ϕ_p = 0.260 wt% the 0.3 contour line is not as well defined as for temperature profile at ΔT_{Bath} = 10˚C.

Implications: Heat transfer characteristics

We can compare this study with other studies and determine how closely derived parameters bear similarities. For example, from Markatos and Pericleous [42], the mean Nusselt number, Nu_H, for an aspect ratio, *A*~1, and a Rayleigh number, Ra_H, defined by $10^6 < Ra_H \leq 10^{12}$ can be derived as:

$$Nu_H = 0.082 Ra_H^{0.329} . \tag{2}$$

Similarly, from Berkovsky and Polevikov [43], Nu_H is also given by for 1 < *A* < 2, set for a Prandtl, *Pr*, range of $10^{-3} < Pr < 10^5$, and if $10^3 < \mathrm{Pr}/(0.2+\mathrm{Pr}))Ra_H (L/H)^3$ then:

$$Nu_H = 0.18\left(\frac{Pr}{0.2+Pr}Ra_H\right)^{0.29}\left(\frac{L}{H}\right)^{-0.13} \tag{3}$$

where Ra_H is based on the height of the convection cell, *H*. The aspect ratio, *A*, was 1.98 for this study. With Nu_H and Ra_H defined as;

$$Nu_H = \frac{1}{H}\int_0^H Nu_y dy \tag{4}$$

$$Ra_H = \frac{g\beta(T_{hot} - T_{cold})H^3}{\nu\alpha} \tag{5}$$

the deviation for this study was 2.54-15.9 % as established from Eq. (2) and 0.11-30.3 % from Eq. (3). The results are summarized in Fig. 7(A). Fig. 7(B) shows local heat transfer coefficients, the local Nusselt numbers, $Nu_{y,\,\mathrm{single}}$ for single-phase natural convection plotted with respect to local Rayleigh numbers, Ra_y, and a trendline of 'Nu_y vs. Ra_y' for single-phase natural convection obtained. The results obtained in this study were compared to analytical data from Churchill and Usagi, [28], Churchill and Chu, [30], and Churchill, [31]. These three correlations are widely accepted and represent the works of numerous studies. From Fig. 7(B), the graph shows three regions as follows: (1) turbulent where $Nu_y = 0.1176Ra_y0^{.3559}$, (2) transition from laminar to turbulent where $Nu_y = 0.2327Ra_y^{0.3053}$, and (3) laminar where $Nu_y = 0.1063Ra_y^{0.3533}$. The transition region is here defined as the range of $1\times10^8 < Ra_y < 1\times10^{10}$. The R-squared values ranged from 0.93 to 0.94 for the transition region, 0.66 for laminar region, and 0.50 for turbulent region. From this study, the values obtained, show relatively higher values compared to Churchill and Usagi, [28], Churchill and Chu, [30], and Churchill, [31]. This is due to thermal stratification within the cell and the fact that the correlations from past studies are for natural convection from a vertical plate in an infinite pool instead of an enclosure with no thermal stratification in bulk temperature. The trendlines obtained from experiments were used as a reference for the determination of the local Nusselt number convection, $Nu_{y,\,\mathrm{two}}$, if any, due to addition of gelatin particles to water.

Consider natural convection heat transfer from an enclosure filled with a stable stratified fluid as shown in Fig**.** 8. The heated wall (hot wall) in the figure is held at constant temperature. An arbitrary bulk temperature profile is shown adjacent to the convection cell. The strength of stratification is measured by the stratification parameter S defined as follows:

$$S = \frac{T_{\mathrm{top}} - T_{\mathrm{bottom}}}{T_{\mathrm{wall,\,y}} - T_{\mathrm{bulk,y}}}, \tag{6}$$

which in the non-stratified case, assumes a value of zero. When an order of magnitude analysis of the conservation equation is performed, the following sets of equations represent steady-state mass, momentum, and energy conservation. From mass conservation equation:

$$\frac{\partial \mathrm{u}}{\partial x} + \frac{\partial \mathrm{v}}{\partial y} = 0 , \tag{7}$$

and:

$$\frac{U}{\delta_{\mathrm{T}}} \sim \frac{V}{H} , \tag{8}$$

where U and V are, respectively, the characteristic velocity in x and y direction, H and δ_{T} are, respectively, the characteristic heated length along the hot wall and thermal boundary layer thickness. From energy equation, then:

$$\mathrm{u}\frac{\partial T}{\partial x} + \mathrm{v}\frac{\partial T}{\partial y} = \alpha \frac{\partial^2 T}{\partial x^2} , \tag{9}$$

and:

$$\frac{V}{H}\Delta T_{\mathrm{x}} + \frac{V}{H}\Delta T_{\mathrm{y}} \sim \frac{\alpha}{{\delta_{\mathrm{T}}}^2}\Delta T_{\mathrm{x}} , \tag{10}$$

where ΔT_{x}, ΔT_{y} are, respectively, the characteristic temperature difference in the x direction and y direction and defined as $\Delta T_{\mathrm{x}} = T_{\mathrm{wall,\,y}} - T_{\mathrm{bulk,y}}$ and $\Delta T_{\mathrm{y}} = T_{\mathrm{top}} - T_{\mathrm{bottom}}$. Using these expressions, Eq. (10) becomes:

$$\frac{V}{H}\left(T_{\mathrm{wall,\,y}} - T_{\mathrm{bulk,y}}\right) + \frac{V}{H}\left(T_{\mathrm{top}} - T_{\mathrm{bottom}}\right) \sim \frac{\alpha}{{\delta_{\mathrm{T}}}^2}\left(T_{\mathrm{wall,\,y}} - T_{\mathrm{bulk,y}}\right) \tag{11}$$

From Eq. (8) therefore:

$$V \sim \frac{\alpha H}{\delta_{\mathrm{T}}{}^{2}}(1+S)^{-1}, \tag{12}$$

where S is stratification parameter as defined in Eq. (6). A similar notation was introduced by Eichhorn et al. [44]. Turning to the momentum equation, then:

$$\mathrm{u}\frac{\partial \mathrm{v}}{\partial x} + \mathrm{v}\frac{\partial \mathrm{v}}{\partial y} = \nu\frac{\partial^2 \mathrm{v}}{\partial x^2} + g\beta\left(T - T_{\mathrm{bulk,y}}\right). \tag{13}$$

The Boussinesq approximation can be made for a fluid phase. The bulk temperature, $T_{\mathrm{bulk,\ y}}$, is a function of y as a result of the stratification. This equation contains three basic groups of terms—inertial term on the left-hand side and viscous diffusion terms plus the buoyancy term on the right-hand side. The three terms that dominate each basic group are:

$$\frac{V^2}{H}, \quad \nu\frac{V}{\delta_{\mathrm{T}}{}^{2}} \quad \sim \quad g\beta\left(T - T_{\mathrm{bulk,y}}\right). \tag{14}$$

Dividing Eq. (14) through by the buoyancy scale $g\beta(T - T_{\mathrm{bulk,y}})$, and using Eq. (12) to eliminate the vertical velocity scale V,

$$\left(\frac{H}{\delta_{\mathrm{T}}}\right)^4 (1+S)^{-2} Ra_{\mathrm{H}}{}^{-1} Pr^{-1}, \quad \left(\frac{H}{\delta_{\mathrm{T}}}\right)^4 (1+S)^{-1} Ra_{\mathrm{H}}{}^{-1} \quad \sim \quad 1 \tag{15}$$

From this expression, it is clear that the competition between inertia and friction is determined by the Prandtl, Pr, number: high-Pr fluids may form a δ_{T} layer ruled by the friction ~ buoyancy balance, while low-Pr fluids may form δ_{T} layer with buoyancy balanced by inertia. Thus;

$$\frac{H}{\delta_{\mathrm{T}}} \sim (1+S)^{1/4} Ra_{\mathrm{H}}{}^{1/4}, \quad \mathrm{Pr} \geq 1, \tag{16}$$

and:

$$\frac{H}{\delta_{\mathrm{T}}} \sim (1+S)^{1/2} Ra_{\mathrm{H}}{}^{1/4} \mathrm{Pr}^{1/4}, \quad \mathrm{Pr} << 1. \tag{17}$$

The term, H/δ_{T} in Eqs. (16) and (17) has a significant meaning. The heat transfer coefficient is defined as:

$$h = \frac{-k(\partial T/\partial x)_{\mathrm{x}=0}}{T_{\mathrm{hot}} - T_{\mathrm{bulk}}}. \tag{18}$$

Introducing the scaling analysis:

$$h \sim \frac{k}{\delta_{\mathrm{T}}} \frac{\Delta T_{\mathrm{x}}}{\Delta T_{\mathrm{x}}} = \frac{k}{\delta_{\mathrm{T}}}, \tag{19}$$

Thus, Nusselt number, *Nu*, is:

$$Nu = \frac{hy}{k} \sim \frac{k}{\delta_T} \frac{H}{k} = \frac{H}{\delta_T}. \tag{20}$$

Therefore, the term H/δ_T is proportional to *Nu*. Eq. (16) and (17) become:

$$Nu \sim (1+S)^{1/4} Ra_H{}^{1/4}, \quad Pr \geq 1, \tag{21}$$

and:

$$Nu \sim (1+S)^{1/2} Ra_H{}^{1/4} \mathrm{Pr}^{1/4}, \quad Pr << 1. \tag{22}$$

For natural convection of ordinary *Pr* fluid ($Pr \geq 1$), then:

$$sNu \equiv \frac{Nu}{(1+S)^{1/4}} \sim Ra_H{}^{1/4}, \tag{23}$$

Where *sNu* is the stratified Nusselt number and where $Pr << 1$ then:

$$sNu \equiv \frac{Nu}{(1+S)^{1/2}} \sim Ra_H{}^{1/4}\,\mathrm{Pr}^{1/4}, \tag{24}$$

with the stratification parameter as a coefficient that modifies the non-stratified Nusselt number and when $S = 0$ then $sNu \sim Nu$. The summary of these relationships is shown in Table 3. We performed an error analysis as discussed in [40] yielding local Nusselt number errors in the range of 0.32 ~ 10.7 %. Fig. 9 shows the variation for particle size of 134 μm and 230 μm. From Fig. 9, at $Ra_y = 10^8$ we can see the laminar to transition region threshold. Also the transition to turbulent region occurs at $Ra_y = 10^{10}$. From Fig. 9 the major difference between two different particle sizes are observed in turbulent region where $10^{10} \leq Ra_y$. The larger the particle size, the lower the value of Nu_y, in turbulent region except for Fig. 9 (C), where the bath temperature difference is 10°C and particle loading is 0.260 wt%. In this case, there is no significant difference when particle size is varied.

Conclusions

Natural convection of a gelatin particle suspension was treated as a two-phase flow with respect to a carrying fluid medium comprising of degassed deionized single-phase water. The heat transfer results revealed that at least four conditions need to be satisfied in part and / or in unison for heat transfer enhancement. The four conditions deemed necessary to induce heat transfer enhancement in a convection cell, as follows:

(1) That a relatively longer particle rise time (lower rise velocity), assuming that the thermal conductivity or thermal capacity of dispersed phase is similar (or larger) than

the continuous phase. This affords time for particles to absorb heat while rising through the boundary layer.

(2) That there is transport of particles from the hot to cold side via buoyancy or convection.

(3) That the rise velocity and rising motion of particles be such that turbulence is induced within the boundary layer; that is, that an exchange of thermally high fluid near the wall and colder fluid be promoted.

(4) That there is a sufficient number and optimum density of particles rising through the boundary layer, such that it makes heat transfer enhancement possible.

Acknowledgments

This study was partially funded by a DOE NEER grant (Grant #: FG07-04ID14592). We immensely appreciate the help of the following: (i) Dan Estel (MST Reactor), (ii) Jason Hall, (iii) affiliated staff at Missouri University of Science and Technology (MST) Reactor facility, and (iv) Dr. David Wronkiewicz for his help.

Nomenclature

Symbol	Description
A	Aspect ratio [H/L]
$\bar{d}$	Number-average particle diameter
d_p	Gelatin particle size (μm)
f_i	Fraction in the class range
g	Gravitational acceleration (m/s^2)
H	Horizontal distance
k	Thermal conductivity (W/m·K)
L	Lateral distance between hot and cold walls
L_1	Thickness of the aluminum tube wall
L_2	Aluminum tape thickness
n_i	Particle quantity
Nu	Nusselt number [hH/k]
Nu_y	Empirically derived (local) Nusselt number [hy/k]
Pr	Prandtl number [ν/α]
q''_x	Heat flux at x (W/m^2)
Ra	Rayleigh number [$g\beta\Delta TH^3/\nu\alpha$]
Ra_H	Rayleigh number with height H [$g\beta\Delta TH^3/\nu\alpha$]
Ra_y	Local Rayleigh number [$g\beta\Delta Ty^3/\nu\alpha$]
S	Stratification parameter [$(T_{top}-T_{bottom})/(T_{wall,y}-T_{bulk,y})$]
S_{ave}	Average stratification parameter
sNu_y	Local stratified Nusselt number [$Nu_y/(1+S)^{1/4}$]
t	Time lapse value between pulses
T	Local temperature in ºC
T_{bottom}	Bulk temperature at the lowest point of the cell (°C)
T_{bulk}	Bulk temperature (°C)
T_{cold}	Temperature of the cold wall (°C)

T_{hot}	Temperature of the hot wall (°C)
T_{inside}	Surface temperature at the inside of the aluminum tube in °C
$T_{surface}$	Surface temperature at the outside of the aluminum tube in °C
ΔT	T_{hot} - T_{cold} (°C)
T_{top}	Bulk temperature at the top (°C)
T_{wall}	Wall temperature (°C)
$\overline{T}_{bulk}$	Bulk temperature determined as an average value in °C
$\overline{T}_{cold}$	Cold wall temperature determined as an average in °C
$\overline{T}_{hot}$	Hot wall temperature determined as an value in °C
u	Perpendicular fluid velocity adjacent to the hot wall
u_p	Particle velocity
v	Fluid velocity component along the hot wall
V	Characteristic velocity in y direction

Greek letters

Symbol	Description
α	Thermal diffusivity (cm^2/s)
β	Thermal expansion coefficient (K^{-1})
σ	Standard deviation
ν	Kinematic viscosity (cm^2/s)

References

[1] Hoffman, A. S., Afrassiabi, A., Dong, L. C., 1986a. Delivery and removal of substances to and from surrounding suspensions using thermally reversible hydrogels. Macromolecular Preprints-IUPAC Macro ’86, 65-66.

[2] Hoffman, A. S., Afrassiabi, A., Dong, L.C., 1986b. Thermally reversible hydrogels; II. Delivery and selective removal of substances from aqueous suspensions. J. Controlled Release 4, 213-222.

[3] Hoffman, A.S., 1987. Applications of thermally reversible hydrogels in therapeutics and diagnostics. J. Controlled Release 6, 297-305.

[4] S. Cui, Y. Hu, Z. Huang, C. Ma, X. Hu., 2014. Cooling performance of bio-mimic perspiration by temperature-sensitive hydrogel. International Journal of Thermal Sciences, Volume 79, 276-282.

[5] Vidyadhar Karlapalem, Subhasisa Rath, Sukanta Kumar Dash, 2019. Orientation effects on laminar natural convection heat transfer from branching-fins. International Journal of Thermal Sciences, Volume 142, 89-105.

[6] Seyed Mohsen Hashem Zadeh, S. A. M. Mehryan, E. Izadpanahi, Mohammad Ghalambaz, 2019, Impacts of the flexibility of a thin heater plate on the natural convection heat transfer. International Journal of Thermal Sciences, Volume 145, Article 106001.

[7] Batchelor, G. K., 1954. Heat transfer by free convection across a closed cavity between vertical boundaries at different temperatures. Quarterly of Applied Mathematics 12, 209-233.

[8] Ming Gao, Ling-shuang Zhang, Da Zhang, Li-xin Zhang, 2019. Experimental study on the enhancement of free convection heat transfer under the action of an electric field. Experimental Thermal and Fluid Science, Volume 104, 9-14.

[9] Ling-peng Kong, Lan Qiao, Yun-yang Xiao, Qing-wen Li, 2019. A study on heat transfer characteristics and pile group influence of enhanced heat transfer energy piles. Journal of Building Engineering, Volume 24, Article 100768.

[10] Jiayue Chen, Zhenqin Xiong, Yao Xiao, Hanyang Gu, 2019. Experimental study on the grid-enhanced heat transfer at supercritical pressures in rod bundle. Applied Thermal Engineering, Volume 156, 299-309.

[11] Zenan Yang, Wei Chen, Minking K. Chyu, 2018. Numerical study on the heat transfer enhancement of supercritical CO2 in vertical ribbed tubes. Applied Thermal Engineering, Volume 145, 705-715.

[12] Rinku Kumar Gouda, Manabendra Pathak, Mohd. Kaleem Khan, 2018. Pool boiling heat transfer enhancement with segmented finned microchannels structured surface. International Journal of Heat and Mass Transfer, Volume 127, Part A, 39-50.

[13] Eckert, E. R. G., Carlson, W. O., 1961. Natural convection in an air layer enclosed between two vertical plates with different temperatures. Int. J. Heat Mass Transfer 2, 106-120.

[14] Elder, J. W., 1965. Laminar free convection in a vertical slot. J. Fluid Mech. 23, part 1, 77-98.

[15] Ostrach, S., 1972. Natural Convection in Enclosures. Advances in Heat Transfer 8, 161-227.

[16] Seki, N., Fukusako, S., Inaba, H., 1978. Visual observation of natural convective flow in a narrow vertical cavity. J. Fluid Mech. 84, 695-704.

[17] Gill, A. E., 1966. The boundary-layer regime for convection in a rectangular cavity. J. Fluid Mech. 26, 515-536.

[18] De Vahl Davis, G., 1968. Laminar natural convection in an enclosed rectangular cavity. Int. J. Heat and Mass Transfer, Vol 11, Issue 11, 1675-1693.

[19] MacGregor, R. K., Emery, A. F., 1969. Free convection through vertical plane layers—Moderate and high Plandtl number fluids. J. Heat Transfer 91, 391-403.

[20] Newell, M. E., Schmidt, F. W., 1970. Heat transfer by laminar natural convection within rectangular enclosures. Journal of Heat Transfer 92, 159-168.

[21] H. Luz Neto, J.N.N. Quaresma, R.M. Cotta, 2002. Natural convection in three-dimensional porous cavities: integral transform method. International Journal of Heat and Mass Transfer, Volume 45, Issue 14, 3013-3032.

[22] H. Luz Neto, J.N.N. Quaresma, R.M. Cotta, 2006. Integral transform solution for natural convection in three-dimensional porous cavities: Aspect ratio effects. International Journal of Heat and Mass Transfer, Volume 49, Issues 23–24, 4687-4695.

[23] Lazaros Elias Mavromatidis, 2016. Study of coupled transient radiation-natural convection heat transfer across rectangular cavities in the vicinity of low emissivity thin films for innovative building envelope applications. Energy and Buildings, Volume 120, 114-134.

[24] De Vahl Davis G, 1986. Numerical Methods in Engineering and Science, George Allen & Unwin, London.

[25] A. K. Datta, S. Yanase, T. Kouchi, M. M. E. Shatat, Laminar forced convective heat transfer in helical pipe flow, International Journal of Thermal Sciences, Volume 120, 2017, Pages 41-49.

[26] J. Zhang, M. Subotic, F. C. Lai, Transient and steady natural convection from a heat source embedded in thermally stratified porous layer, International Journal of Thermal Sciences, Volume 49, Issue 9, 2010, Pages 1527-1535.

[27] Eckert, E. R. G., Drake, Jr. R. M., 1972. Analysis of heat and mass transfer. McGraw-Hill.

[28] Churchill, S. W., Usagi, R., 1972. A general expression for the correlation of rates of transfer and other phenomena. ALChE Journal 18, 1121-1128.

[29] Churchill, S. W., Ozoe, H., 1973. A correlation for laminar free convection from a vertical plate. Journal of Heat Transfer, 540-541.

[30] Churchill, S. W., Chu, H. H. S., 1975. Correlating equations for laminar and turbulent free convection from a vertical plate. Int. J. Heat Mass Transfer 18, 1323-1329.

[31] Churchill, S. W., 1983. Free convection around immersed bodies. Heat exchanger design handbook, Schlünder, E. U. (ed.), Hemisphere, New York.

[32] Jaluria, Y., 1987. Basics of natural convection; Handbook of single-phase convective heat transfer: Kakaç, S., Shah, R. K., Aung, W. (eds.), Wiley, New York.

[33] Gebhart, B, Jaluria, Y., Mahajan, R. L., Sammakia, B., 1988. Buoyancy-induced flows and transport. Hemisphere, New York.

[34] Lykoudis, P. S., Tokuhiro, A. T., 1990. Natural convection over a vertical heated flat plate with gas injection and in the presence of a magnetic field. Proc. 6th Beer-sheva Int. Sem. MHD Flows and Turbulence, AIAA Publishing.

[35] Rahman, S., 1995. Food properties handbook. CRC Press.

[36] Phelps, G. W., 1958**,** Particle size analysis: theoretical and practical aspects: United Clay Mines Corporation.

[37] Jelínek, K. Z., 1974. Particle size analysis Translation editor: Bryce, W. A. J., (ed.), Halsted Press New York

[38] Barth, H. G., (ed.) 1984. Modern methods of particle size analysis. Wiley, New York.

[39] I. Hagiwara, A. Tokuhiro, P. G. Oduor, 2014. Natural convection heat transfer of hydrophilic particle suspension: Implications on nuclear waste remediation, International Journal of Heat and Mass Transfer, Volume 78, 636 – 647.

[40] I. Hagiwara, A. Tokuhiro, P. G. Oduor, 2015. Comparison between Single- and Two-Phase Heat Transfer in a Thermally Stratified Enclosure, International Journal of Thermal Sciences, 2015, Volume 92, 173 – 178.

[41] Bejan, A., 2013. Convection heat transfer. 4th ed., Wiley, New York. 685 p.

[42] Markatos, N. C., Pericleous, K. A., 1984. Laminar and turbulent natural convection in an enclosed cavity. Int. J. Heat Mass Transfer 27, 755-772.

[43] Berkovsky, B. M., Polevikov, V. K., 1976. Numerical study of problems on high-intensive free convection. Heat transfer and turbulent buoyant convection, volume II, Spalding, D. B., Afgan, N. (ed.), McGraw-Hill, New York.

[44] Eichhorn, R., Lienhard, H. H., Chen, C. C., 1974. Natural convection from isothermal spheres and cylinders immersed in a stratified fluid. Fifth International Heat Transfer Conference, Tokyo, NC1.3, 10-14.

List of Figures

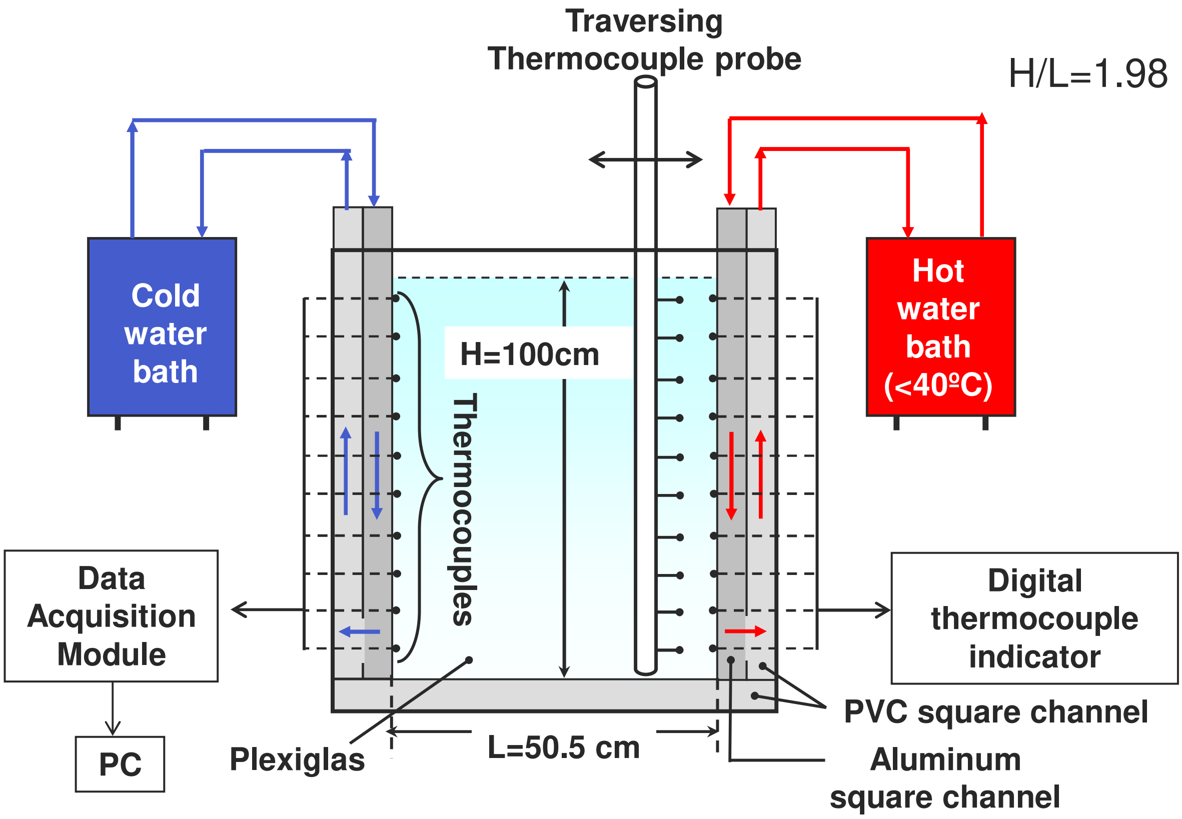

Figure 1: Schematic diagram of experimental setup.

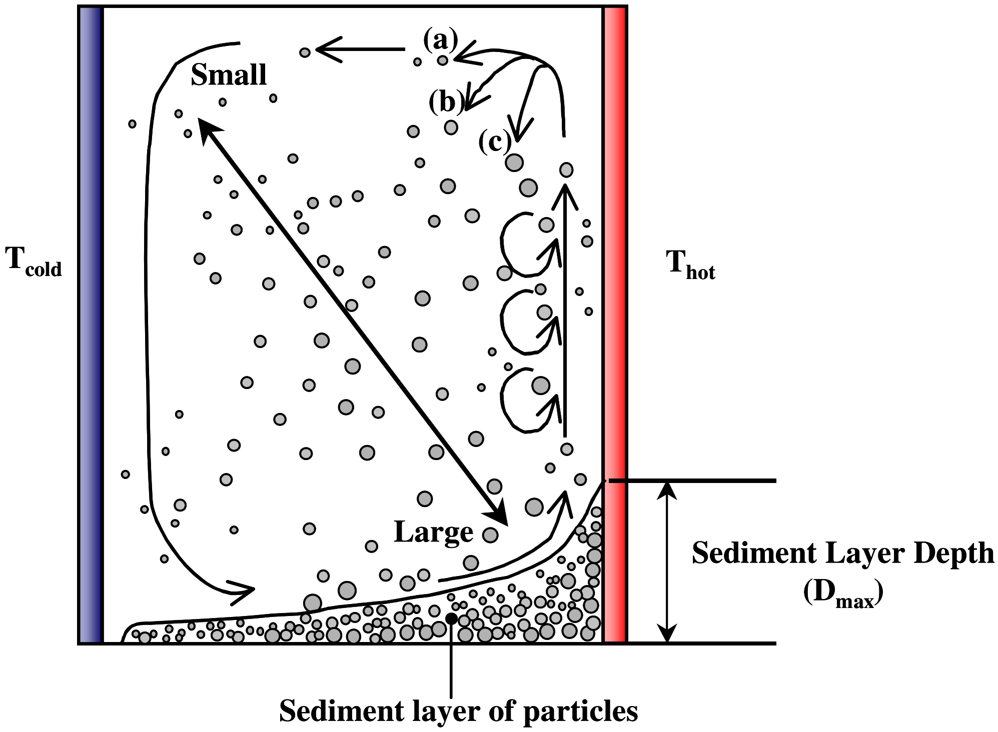

Figure 2. Schematic illustration of sedimentation of gelatin particles.

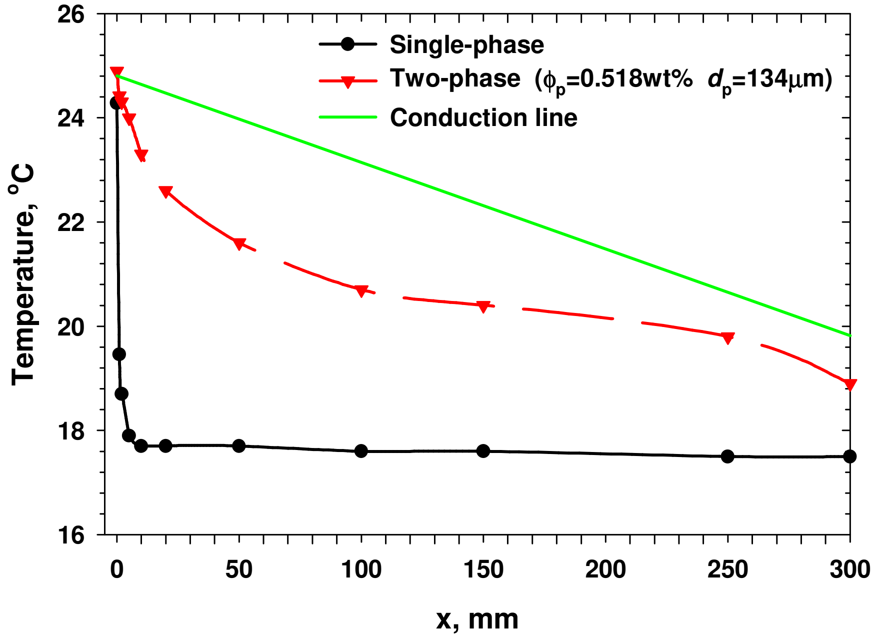

Figure 3. Temperature profiles at 3.0 cm from bottom of the cell for both single-phase and two-phase for bath temperature difference of 10 °C. The two-phase profile shows the effect of sedimentation on temperature within this region.

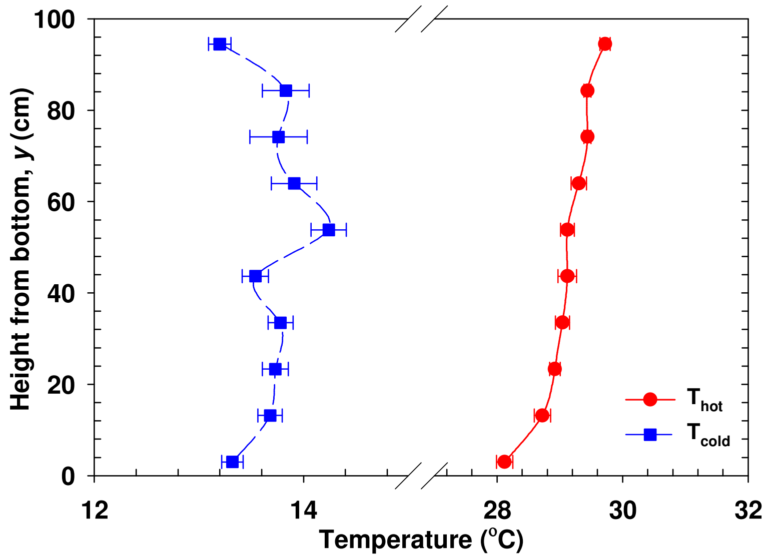

Figure 4. Wall temperature distribution for single-phase. The results displayed are from the 8th experimental run.

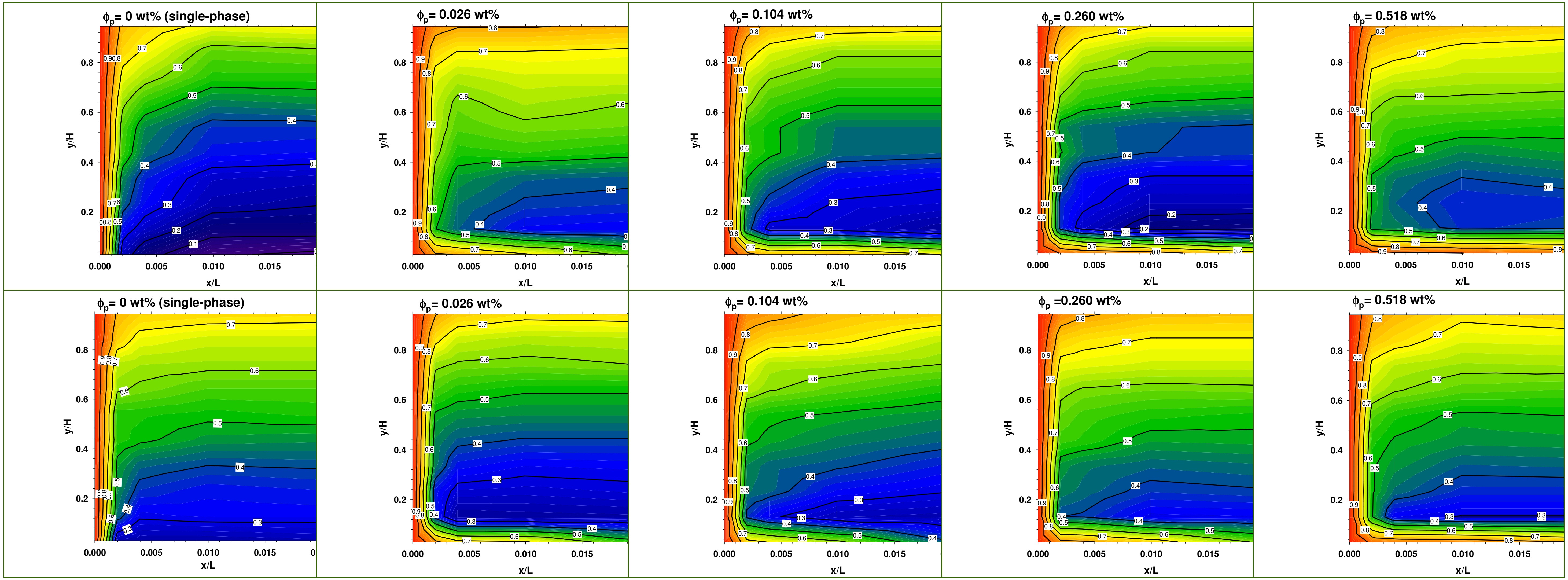

Figure 5. (A). Top row shows temperature contours for single- and two-phase flow for particle size of 134 μm at ΔT_{Bath}= 10°C for various particle loadings at near the hot wall ($0 \leq x/L \leq 0.02$). (B). Bottom row shows temperature contours for single- and two-phase flow for particle size of 134 μm at ΔT_{Bath}= 20°C for various particle loadings at near the hot wall ($0 \leq x/L \leq 0.02$).

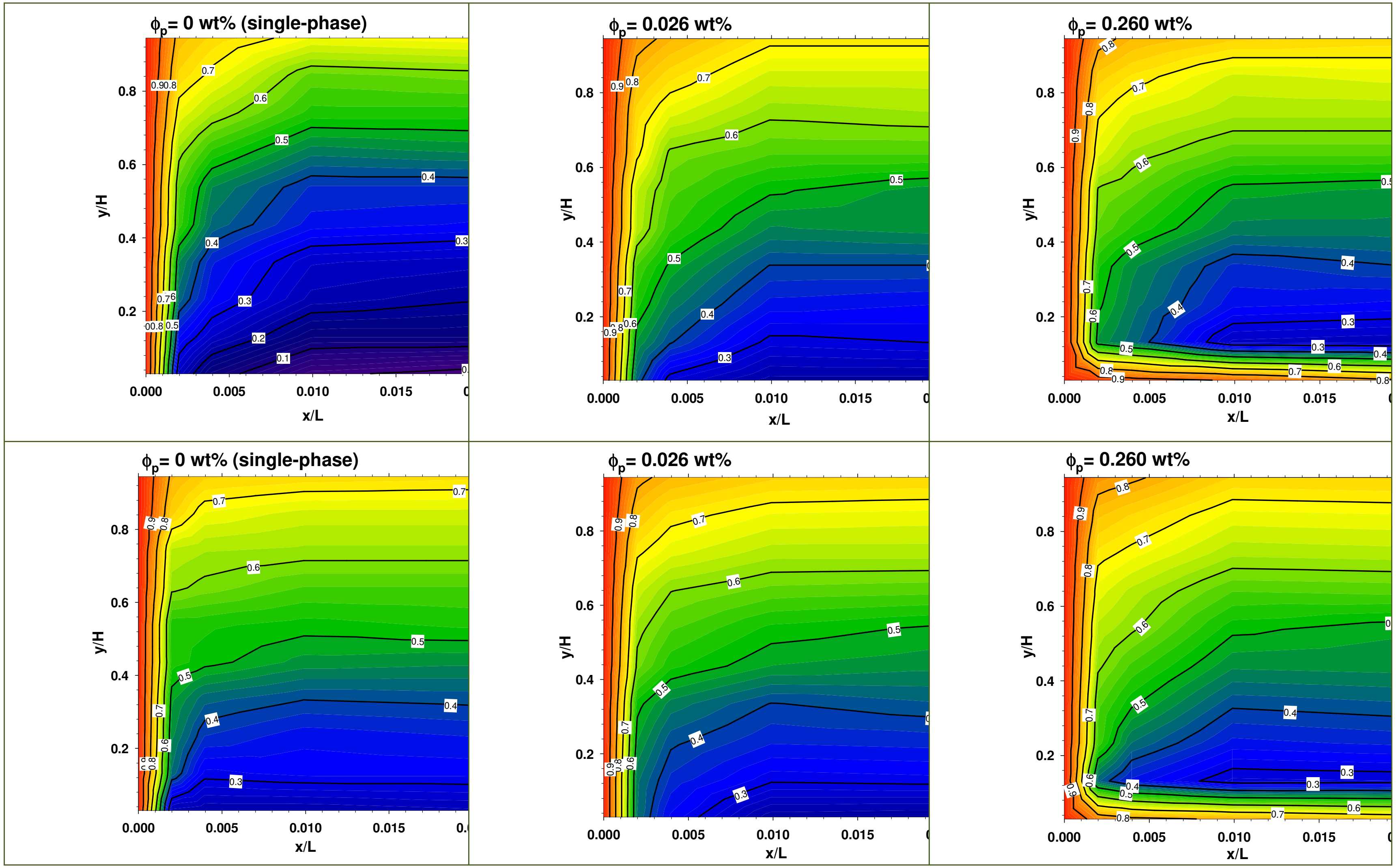

Figure 6. (A). Temperature contours for gelatin particle size of, d_2 = 230 μm. at ΔT_{Bath} = 10˚C at near the hot wall ($0 \le x/L \le 0.02$). (B). Bottom row shows temperature contours for gelatin particle size of, d_2 = 230 μm. at ΔT_{Bath} = 20˚C at near the hot wall ($0 \le x/L \le 0.02$).

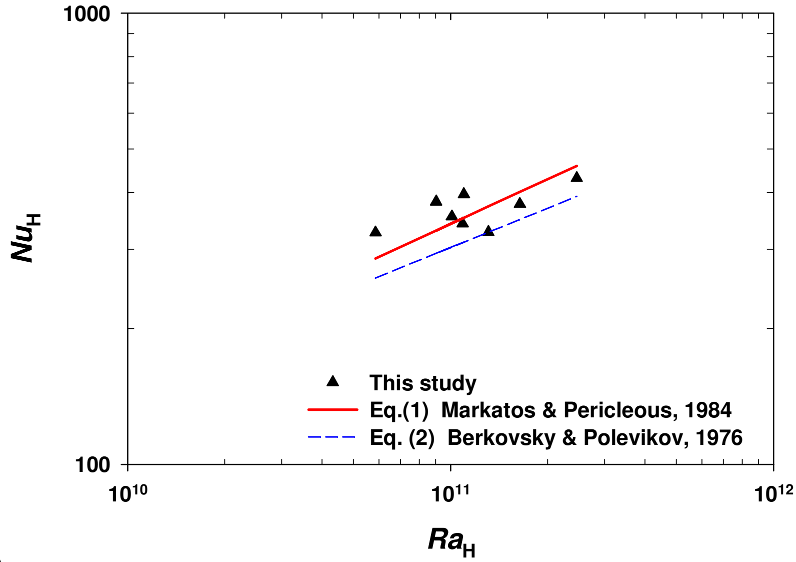

A B

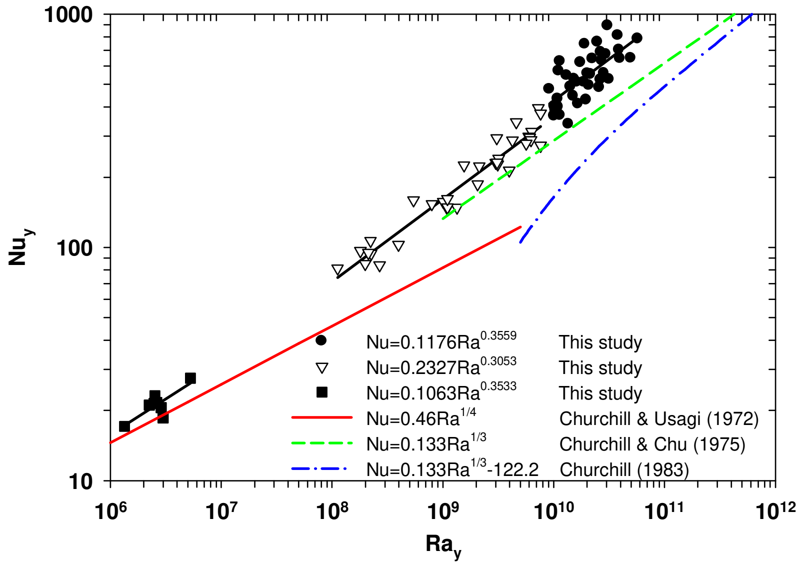

Figure 7. Comparison of Eq. (1) and (2) with experimental data for single-phase natural convection in enclosures. Graph of Nusselt numbers against Rayleigh numbers for the single-phase flow. The graphs are compared to data obtained from various authors. From this study, the values obtained, show relatively higher values compared to Churchill and Usagi, [28], Churchill and Chu, [30], and Churchill, [31].

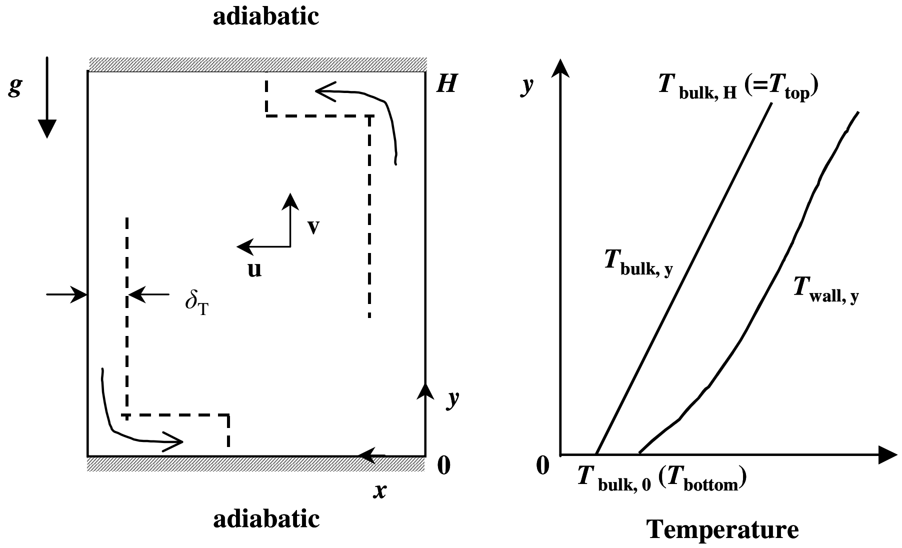

Figure 8. Natural convection in an enclosure filled with thermally stratified fluid and bulk and wall temperature distribution.

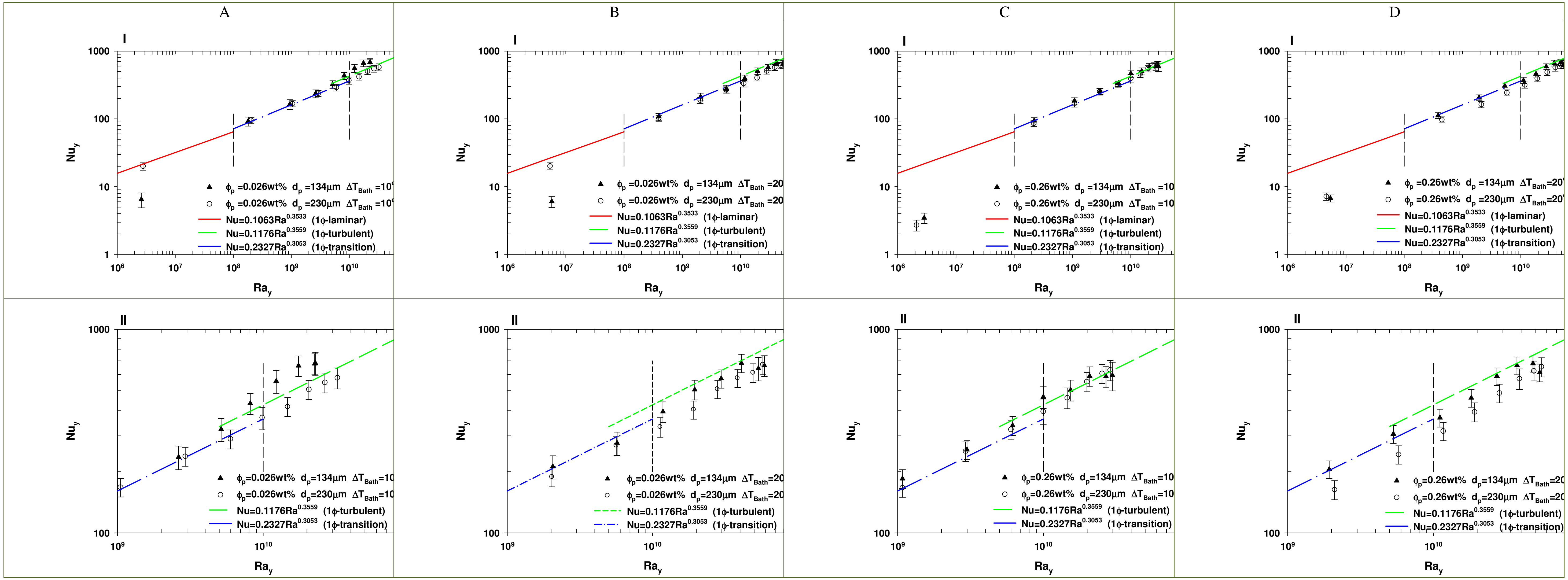

Figure 9. Graph of Nusselt numbers against Rayleigh numbers for the two-phase flow. (A) (I) shows the variation for particle size of 134 μm and 230 μm for bath temperature difference of 10°C. The particle loading is 0.026 wt%. (II) is an enlargement of (I) from $10^9 \leq Ra_y \leq 10^{11}$ and $100 \leq Nu_y \leq 1000$. The decrease in Nusselt number is seen at the lower Rayleigh number, $10^6 \leq Ra_y \leq 10^7$ for case of particle size of 134 μm. The lower the particle loading, the lower the value of Nu_y in turbulent region. (B) (I) shows the variation for particle size of 134 μm and 230 μm for bath temperature difference of 20°C. The particle loading is 0.026 wt%. (II) is an enlargement of (I) from $10^9 \leq Ra_y \leq 10^{11}$ and $100 \leq Nu_y \leq 1000$. The decrease in Nusselt number is seen at the lower Rayleigh number, $10^6 \leq Ra_y \leq 10^7$, for case of particle size of 134 μm. The lower the particle size, the lower the value of Nu_y in turbulent region. (C) (I) shows the variation for particle size of 134 μm and 230 μm for bath temperature difference of 10°C. The particle loading is 0.26 wt%. (II) is an enlargement of (I) from $10^9 \leq Ra_y \leq 10^{11}$ and $100 \leq Nu_y \leq 1000$. The decrease in Nusselt number is seen at the lower Rayleigh number, $10^6 \leq Ra_y \leq 10^7$. There is no significant difference when particle size is varied. (D) (I) shows the variation for particle size of 134 μm and 230 μm for bath temperature difference of 20 °C. The particle loading is 0.26 wt%. (II) is an enlargement of (I) from $10^9 \leq Ra_y \leq 10^{11}$ and $100 \leq Nu_y \leq 1000$. The decrease in Nusselt number is seen at the lower Rayleigh number, $10^6 \leq Ra_y \leq 10^7$. The lower the particle size, the lower the value of Nu_y.

List of Tables

Table 1. Mean sediment layer depth for two-phase runs.

Run Number	Temperature difference, ΔT_{Bath} (ºC)	Particle diameter, d_p (μm)	Particle loading, ϕ_p (wt%)	D_{max} (cm)	Mean sediment layer depth, $\overline{D}$ (cm)
9	10	134	0.026	3.0*	-
10	20	134	0.026	3.0*	-
11	10	134	0.104	4.0	3.1
12	20	134	0.104	5.0	2.0
13	10	134	0.26	7.5	6.0
14	20	134	0.26	12	2.9
15	10	134	0.518	13.2	11.3
16	20	134	0.518	10.0	3.7
17	10	230	0.026	3.0	1.6
18	20	230	0.026	1.7	1.2
19	10	230	0.26	14.0	9.4
20	20	230	0.26	14.0	10.5

* For 9th and 10th experimental runs, the sediment layer depth was measured only at the center of the experimental cell.

Table 2. Wall temperature distribution.

Run	$\overline{T}_{hot}$ (˚C)	$T_{h, max}$ (˚C)	$T_{h, min}$ (˚C)	ΔT_h (˚C)	Difference (%)	$\overline{T}_{cold}$ (˚C)	$T_{c, max}$ (˚C)	$T_{c, min}$ (˚C)	ΔT_c (˚C)	Difference (%)
1	24.83	24.96	24.39	0.57	2.30	21.55	21.75	21.42	0.33	1.53
2	24.26	24.71	23.07	1.64	6.76	16.98	17.32	16.80	0.52	3.06
3	24.84	25.1	24.58	0.52	2.09	18.53	18.76	18.33	0.43	2.32
4	24.30	24.82	23.9	0.92	3.79	18.69	18.98	18.51	0.47	2.52
5	24.63	24.84	24.28	0.56	2.28	17.71	18.00	17.47	0.53	3.00
6	23.90	24.61	22.04	2.57	10.75	14.15	14.56	13.81	0.75	5.30
7	24.04	24.88	22.00	2.88	11.96	8.59	8.97	8.04	0.93	10.83
8	29.09	29.72	28.12	1.6	5.50	13.70	14.24	13.20	1.04	7.58

The maximum temperature difference for the hot wall temperature was 12.0 % and for the cold wall was 10.8 %. As it is seen in the table, the temperature difference along the wall, ΔT_h (ΔT_c), increases as the temperature difference between the hot and cold wall, $\overline{T}_{hot} - \overline{T}_{cold}$, increases. This is due to the fact that the bulk temperature difference between the top and bottom of the cell becomes larger as the temperature difference between the hot and cold wall increases.

Table 3. Summary of *Nu-Ra* relationships.

Nu-Ra correlation	Prandtl number limitation	Stratified/non-stratified
$Nu \sim Ra^{1/4}$	$Pr \geq 1$	$S = 0$
$Nu \sim (Ra \cdot Pr)^{1/4}$	$Pr << 1$	$S = 0$
$Nu \sim (1+S)^{1/4} Ra^{1/4}$	$Pr \geq 1$	$S \geq 0$
$Nu \sim (1+S)^{1/2} (Ra \cdot Pr)^{1/4}$	$Pr << 1$	$S \geq 0$